PLANETARY CRATER DETECTION AND REGISTRATION USING MARKED POINT PROCESSES, MULTIPLE BIRTH AND DEATH ALGORITHMS, AND REGION-BASED ANALYSIS

David Solarna[2], Gabriele Moser[2], Jacqueline Le Moigne[1], Sebastiano B. Serpico[2]

[1] NASA Goddard Space Flight Center, Greenbelt, MD 20771, jacqueline.j.lemoigne-stewart@nasa.gov
[2] University of Genoa, DITEN Dept., Via Opera Pia 11a, 16145 Genoa, Italy, gabriele.moser@unige.it

ABSTRACT

Because of the large variety of sensors and spacecraft collecting data, planetary science needs to integrate various multi-sensor and multi-temporal images. These multiple data represent a precious asset, as they allow the study of targets' spectral responses and of changes in the surface structure; because of their variety, they also require accurate and robust registration. A new crater detection algorithm, used to extract features that will be integrated in an image registration framework, is presented. A marked point process-based method has been developed to model the spatial distribution of elliptical objects (i.e. the craters) and a birth-death Markov chain Monte Carlo method, coupled with a region-based scheme aiming at computational efficiency, is used to find the optimal configuration fitting the image. The extracted features are exploited, together with a newly defined fitness function based on a modified Hausdorff distance, by an image registration algorithm whose architecture has been designed to minimize the computational time.

Index Terms— Marked Point Processes, Crater Detection, Region-based Analysis, Image Registration, Hausdorff Distance

1. INTRODUCTION

Planetary science is continuously evolving, and with new science and exploration goals, large amounts of data need to be analyzed and integrated. In this field, data heterogeneity is highly present and it is an issue to deal with. Sensors collecting images have different characteristics, such as different resolutions or different operating spectra; moreover, they do not always operate under the same conditions, and images of the same area may be different because of different illumination or acquisition time. Since images have to be aligned in the same reference system to be compared and analyzed, one of the primary needs is image registration; automatic and robust processing techniques need to be used, since manual operations are time consuming and, due to the increase of planetary data sets, registration needs to be automated. In this paper, the registration of planetary images is addressed by a two-stage approach: first, craters are detected by using a marked point process (MPP) model optimized through a birth-death sampling process; then, registration is accomplished by matching the extracted craters through the optimization of distance and information-theoretic functions.

2. METHODOLOGY

2.1. Overview of the Method

A newly designed crater detection algorithm is used as a feature extraction method for image registration. The algorithm developed here is based on an MPP model. Image registration is performed in two steps. First, crater-based features are used, together with a similarity measure based on a modified Hausdorff distance, to quickly find an approximated solution. Its neighborhood is then searched for by a second registration step based on a mutual information-based similarity measure.

2.2. Marked Point Process Model

We model the distribution of craters on a planetary surface by a realization of an MPP, x. An MPP [1] is an abstract random variable whose realizations are configurations of objects, each one being described by a marked point. Similar to Markovian modeling, the maximum-a-posteriori (MAP) criterion can be proved to be equivalent, under MPP assumption, to the minimization of a suitable energy function. The energy function has to be designed to take into account the interactions between the geometric objects and the way they fit the image.

Each crater is described by a 5-tuple (u_0, v_0, a, b, θ). The first two components represent the center $C = (u_0, v_0)$ of the ellipse (i.e. one point belonging to the realization of the point process), while the other three are the marks and correspond to the major axis, the minor axis, and the orientation (Figure 1). The 5-tuple takes values from:

$$S = [0, M] \times [0, N] \times [a_m, a_M] \times [b_m, b_M] \times [0, \pi],$$

where $M \times N$ is the image size, $[a_m, a_M]$ is the range for the major axis, $[b_m, b_M]$ is the range for the minor axis, and $[0, \pi]$ is the set of all the possible orientations.

2.3. Definition of the Energy Function

The best configuration of ellipses is estimated on the basis of the contour map extracted with an edge detection algorithm like Canny's. Since a Gibbs formulation is proven to hold for

the posterior distribution of the realization x conditioned to the contour map I_g, a density function f_p can be defined as follows [2]:

$$f_p(x|I_g) \propto exp\left(-U(x|I_g)\right)$$

where the energy function $U(x|I_g)$ has to be defined according to the problem at hand. It is made up of two terms, a prior term $U_P(x)$ that takes into account the interactions between the geometric objects $x_1, \dots, x_n$ (each formalized as a 5-tuple) in the configuration $x = \{x_1, \dots, x_n\}$ of n ellipses (n craters), and a likelihood term $U_L(x|I_g)$ describing the way the ellipses fit the contour map. The second term is divided, in turn, into two contributions: $U_S(x|I_g)$ and $U_D(x|I_g)$ (see below). Moreover, since a realization x is made of n ellipses, it is convenient to associate, whenever possible, an energy contribution to each i-th ellipse and write the total configuration energy as:

$$U(x|I_g) = \sum_i U_P^i(x_i) + U_S^i(x_i|I_g) + U_D^i(x_i|I_g)$$

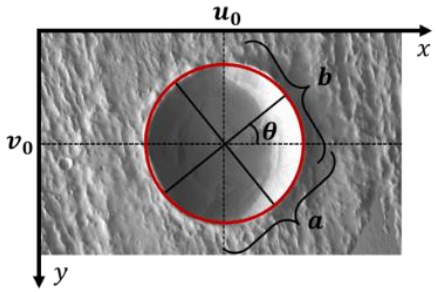

Figure 1: Example of a crater modeled as an ellipse.

2.3.1. Prior Term

The prior term characterizes the general aspect of the desired solution. Two overlapping craters are very unlikely, so the energy term U_P adds a repulsion coefficient to the total energy if the i-th ellipse intersects any of the other ellipses in the configuration:

$$U_P^i(x_i) = \frac{1}{n} \sum_{x_i \cap x_j > 0} R(x_i, x_j), \qquad R(x_i, x_j) = \frac{x_i \cap x_j}{x_i \cup x_j}$$

where $R(x_i, x_j)$ is the repulsion coefficient between the two ellipses x_i and x_j, $x_i \cap x_j$ is the overlapping area, and $x_i \cup x_j$ is the union of the areas.

2.3.1. Likelihood Term

The first of the two terms that contribute to the definition of the likelihood energy is a correlation measure. It represents the similarity between the object x_i in the configuration x and the data I_g by computing a sort of correlation coefficient between the extracted and the modeled edges:

$$U_S^i(x_i|I_g) = -\frac{\left\|\{(u,v): I_g(u,v) = 1 \,\&\, \Pi(u,v|x_i) = 1\}\right\|}{\left\|\{(u,v): I_g(u,v) = 1\}\right\|}$$

where $\|A\|$ indicates the cardinality of the set A (i.e. the number of elements in A), (u, v) are the coordinates of a point in the image plane, and $\Pi(\cdot\,|x_i)$ is the outline of the object x_i in the image plane. The minus sign is included so that minimizing the energy favors maximizing the correlation.

The term U_D^i measures the distance between the ellipse x_i in the configuration and the contours of the data. It is determined by the Hausdorff distance $d_H(x_i, I_g)$ between the sets of points such that $\Pi(u, v|x_i) = 1$ and those such that $I_g(u, v) = 1$:

$$U_D^i(x_i|I_g) = \frac{1}{n} \frac{d_H(x_i, I_g)}{a_i}$$

where the major axis a_i of the ellipse x_i is used as a normalization term to avoid unbalanced terms related to small and big ellipses in the total energy.

2.4. Multiple Birth and Death Algorithm

For the minimization of the energy function, a Markov Chain Monte Carlo (MCMC) algorithm [3], coupled with a simulated annealing (SA) scheme, is used. The minimization is carried out with respect to the locations, the marks, and the number of the ellipses. In particular, the MPP X is sampled by using a multiple birth and death (MBD) algorithm. It allows building a Markov chain $X_k(k = 0,1, \dots)$ in the space of all possible configurations, which, in the ideal case, ergodically converges to the optimum distribution [4]. MBD, after an initialization step, iterates through birth and death steps embedded in a probabilistic framework [5]:

- **Initialization:** Regarding the SA, there are two parameters to be set. The first is the inverse of the temperature β, while the second is the discretization step δ. They are set at an initial value of $\beta = 50$ and $\delta = 200{,}000$ respectively, and they evolve according to a geometric scheme of reason $k = 0.97$ through the iterations. The values have been chosen according to the MPP literature [6]. The initialization step also generates the birth map $b(s)$, a pdf describing in which pixels $s = (u, v)$ are more probable to find craters, useful to speed up the convergence. The pdf is generated by finding possible ellipses centers using a generalized Hough accumulator [7]. The centers are then used as seeds points to be spread through a Gaussian filtering.
- **Birth Step:** At each iteration, new objects are added to the configuration according to the birth map defined above and to the temperature parameter defined for the SA scheme. For every pixel s in the image I, a new ellipse is added with probability $B(s) = min\{1, \delta \cdot b(s)\}$.
- **Death Step:** The goal of the death step is to reduce the list of objects in the configuration returned by the birth step according to a probability term based on the energy values of all the objects. First, for every ellipse in the configuration the likelihood term is computed and the objects are killed with probability $d(x_i)$:

$$d(x_i) = \frac{\delta \cdot a(x_i)}{1 + \delta \cdot a(x_i)},$$

where:

$$a(x_i) = e^{-\beta\left(U_L(\{x \setminus x_i\}|I_g) - U_L(x|I_g)\right)} = e^{\beta \cdot U_L^i(x_i|I_g)}$$

Then, the survived configuration is analyzed and among the overlapping ellipses, identified by a high prior energy term, only the ones with lower death probability are kept in order to grant the desired configuration.

- **Convergence Test:** The algorithm stops sampling the process when the ellipses that are killed in the i-th iteration are exactly the same ones that were born in the same iteration. In order to check that the simulated annealing is freezing the result into the desired minimum, the algorithm stops only if the numbers of the new objects and of the killed ones are smaller than 5% of a predefined maximum.

2.5. Region-based Approach

MBD is computationally heavy, and the computational burden increases with the image size. Because of that, working with planetary data can be a problem, thus a region-based solution was developed. A set of rectangular regions are extracted from the image and MBD is run in parallel on each region. The results obtained this way are then aggregated back into the reference system of the original image. The segmentation process is based on the thresholding of the birth map. A set of connected components is extracted from the thresholded birth map and the method of moments is applied to them in order to find their centroids and axes. This information is used to define the regions by creating rectangles as bounding boxes for the connected components. The centers of the rectangles correspond to the centroids, while the sizes of the regions are obtained from the major axes.

2.5. Image Registration

Given two planetary images, let us choose one as the reference image and the other as the input image to be registered.

The mapping is modeled as a rotation-scale-translation (RST) transformation and is parametrized by a vector $p = (t_x, t_y, \theta, k)$, where $\{t_x, t_y\}$ denote translation in the x and y directions, θ is the rotation angle, and k is the scaling factor. The crater detection algorithm is used in the registration process as the feature extraction method: craters are extracted from the reference and the input images and the optimal RST transformation is computed through the optimization, with respect to p, of the Hausdorff distance between the outlines of the craters in the two images.

To favor both accuracy and computational efficiency of the registration process, we adopted a two-step procedure. A first solution is found by using the aforementioned similarity measure based on the Hausdorff distance between the extracted craters. This method is fast, as the measure is not computationally heavy since the sets of points are small, but its accuracy depends on the performance of the crater detection algorithm. To overcome this shortcoming, a second step registration based on the mutual information is also applied on the intensity values in a neighborhood of the first solution. This second step is fast, as the search space has been dramatically reduced by the previous stage, and is also accurate, as registration based on this mutual information measure is known to be robust and effective [8]. The result is an image registration scheme granting the speed properties of the crater-based registration with the accuracy of the mutual information-based technique. A genetic algorithm has been used for the minimization of the two similarity measures [9]

3. EXPERIMENTAL RESULTS

3.1. Data Set

For the performance assessment of the crater detection algorithm we have used 13 images collected on the surface of Mars by the Thermal Emission Imaging System (THEMIS) and the High Resolution Stereo Camera (HRSC) sensors. The former has 5 visible bands at 18-m resolution, and 10 infrared bands at 100-m resolution, while the latter has 2.3-m resolution.

To validate the proposed registration method, we have followed two approaches. First, to allow quantitative assessment, we have generated semi-synthetic data sets (starting from the aforementioned images) endowed with ground truth. Then, we have also tested the method on real multi-temporal data representing the landing site of the Apollo 17 spacecraft on the Moon's surface, and evaluated the results visually.

3.2. Crater Detection

A quantitative assessment of the results obtained by the proposed crater detection method was accomplished by computing the detection percentage D, the branching factor B, and the quality percentage Q:

$$D = \frac{TP}{TP + FN}; \quad B = \frac{FP}{TP}; \quad Q = \frac{TP}{TP + FP + FN}$$

where true positives (TP), false positives (FP), and false negatives (FN) refer to numbers of target objects (the craters) and not to pixel counts. Table I reports the average values of these performance parameters for the THEMIS, the HRSC, and all 13 considered images. The smallest image is 1581×1827 pixels, while the largest is 2950×5742. On a 2,3GHz quad-core processor the computational time ranges from tens of minutes to less than an hour. The results confirm that the proposed method was effective in detecting the craters in the input images with low false-alarm rates.

Visual examples of the results are shown in Figure 2 and confirm the accurate detection of the craters in the imaged scenes. The proposed method was compared to another crater

detection algorithm [1], and resulted in more effective performances for all three measures.

3.3. Image Registration

The performance assessment is based on the computation of the Root Mean Square (RMS) error [10]. Table II summarizes the RMS errors on the semi-synthetic data sets generated from THEMIS and HRSC images by simulating an RST transformation and adding zero mean Gaussian noise.
Subpixel accuracy is obtained by the proposed approach thanks to the combination of feature-based (Hausdorff) and area-based (mutual information) registration stages. The usage of the second step registration improves the RMS error of 0.4 on average. The visual results obtained with real multi-temporal data sets collected by the Lunar Reconnaissance Orbiter Camera (LROC) are presented in Figure 3 in a checkerboard visualization. The reference and the registered input images are shown together in adjacent squares.

4. CONCLUSIONS

Our novel crater detection algorithm has been proven to achieve very interesting performance allowing to obtain accurate crater maps useful for both image registration and planetary science studies. With regards to image registration, sub-pixel accuracy is achieved and measured precisely using semi-synthetic data sets. In future work, it would be interesting to apply this new method to other applications requiring the extraction of ellipsoidal or circular features, as for example the processing and the registration of medical images. It would be also interesting to test the registration algorithm on additional multi-temporal or multi-sensor data sets, with corresponding ground truth provided by the users, to assess the robustness provided by the crater detection algorithm.

ACKNOWLEDGEMENT

The authors would like to acknowledge Brent Garry, NASA Goddard Space Flight Center, for providing the LROC data.

5. REFERENCES

[1] G. Troglio, J. A. Benediktsson, G. Moser and S. B. Serpico, "Crater Detection Based on Marked Point Processes," *Signal and Image Processing for Remote Sensing*, pp. 325-338, 2012.

[2] M. Ortner, X. Descombes and J. Zerubia, "A marked point process of rectangles and segments for automatic analysis of digital elevation models," *IEEE Transactions on Pattern Analysis and Machine Intelligence*, vol. 30, p. 105–119, 2008.

[3] C. Geyer, "Likelihood inference for spatial point processes," *Stochastic Geometry: Likelihood and Computation*, pp. 79-140, 1999.

[4] C. Robert and G. Casella, Monte-Carlo Statistical Methods, New York: Springer-Verlag, 1999.

[5] X. Descombes, R. Minlos and Z. E. J., "Object Extraction Using a Stochastic Birth-and-Death Dynamics in Continuum," *Journal of Mathematical Imaging and Vision*, vol. 33, pp. 347-359, 2009.

[6] E. Zhizhina and X. Descombes, "Double Annealing Regimes in the Multiple Birth-and-Death Stochastic Algorithms," *Markov Process and Related Fields*, vol. 18, pp. 441-456, 2012.

[7] G. Troglio, J. Le Moigne, J.A. Benediktsson, G. Moser, and S.B. Serpico, "Automatic Feature Extraction from Planetary Images," *IEEE Geoscience and Remote Sensing Letters*, Vol. 9, No. 1, pp. 95-99, January 2012.

[8] J. Le Moigne, N. S. Netanyahu and R. D. Eastman, Image Registration for Remote Sensing, Cambridge University Press, 2011.

[9] G. Troglio, J. Benediktsson, S. Serpico, G. Moser, R. Karlsson, G. Halldorsson and E. Stefansson, "Automatic Registration of Retina Images based on Genetic Techniques," in *International IEEE EMBS Conference*, Vancouver, 2004.

[10] I. Zavorin and J. Le Moigne, "Use of multiresolution wavelet feature pyramids for automatic registration of multisensor imagery," *IEEE Transactions on Image Processing*, vol. 14, no. 6, pp. 770-782, 2005.

Table I. Average accuracy parameters of the MPP-based Crater Detection Algorithm

Data	D	B	Q
THEMIS images	0.91	0.10	0.83
HRSC images	0.89	0.06	0.85
Average on all 13 images	0.90	0.09	0.84

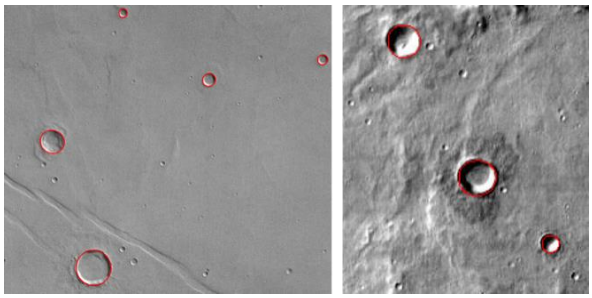

Figure 2: Results obtained from applying the crater detection algorithm to an HRSC (right) and a THEMIS (left) image

Table II. RMS error of the Registration Algorithm

Data	RMS Error
THEMIS (10 data sets)	0.31
HRSC (10 data sets)	0.22
Average (20 data sets)	0.26

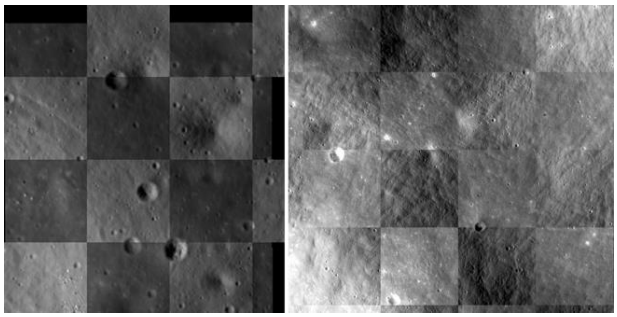

Figure 3: Registration results for the real data sets.